PHOTODISINTEGRATION OF THE DEUTERON FROM 500 TO 900 MEV

Thesis by

Henry Richard Myers

In Partial Fulfillment of the Requirements

For the Degree of

Doctor of Philosophy

California Institute of Technology

Pasadena, California

1960

ACKNOWLEDGMENTS

This experiment was suggested and supervised by Dr. Alvin V. Tollestrup whose instruction and advice throughout the author's graduate residence are sincerely appreciated.

Gratitude is expressed to Dr. Ricardo Gomez for his interest and participation in this project. The contributions of Mr. Daniel Guinier in the construction and data taking phases of the experiment were most helpful. Dr. Robert F. Christy was responsible for several valuable discussions concerning the interpretation of the data. The interest of Dr. Robert F. Bacher is appreciated.

The liquid deuterium target was maintained by Mr. Earle B. Emery. Messers. Lawrence B. Loucks, Daniel D. Sell, Alfred A. Neubeiser, Lucien Luke and the synchrotron crew were of continuous assistance.

Financial support was provided in part by the United States Atomic Energy Commission.

ABSTRACT

The reaction $\gamma + D \rightarrow P + N$ has been studied for photon energies between 500 and 900 mev. Bremsstrahlung from the California Institute of Technology electron synchrotron interacted in a liquid deuterium target. A measurement of the energy and angle of the protons arising in such interactions was sufficient to establish that photodisintegration without pion emission had occurred and to determine the energy of the photon which gave rise to the detected proton. An excitation curve was obtained at 90° in the laboratory and angular distributions were measured for photon energies of 500 and 700 mev. The results imply a total cross section which decreases from 7 μb at 500 mev to 1 μb at 900 mev.

TABLE OF CONTENTS

I

INTRODUCTION

The simplest and most informative photonuclear reactions in energy regions below the meson threshold are proton Compton scattering and photodisintegration of the deuteron. In the region just above the photodisintegration threshold the latter process provides a useful complement to the low energy n-p scattering and radiative capture experiments. For these energies the matrix elements for photodisintegration depend on the electric and magnetic multipole moments for transitions between initial and final states of the n-p system and results are independent of the detailed shape of the deuteron potential. Also, since the dipole approximation is valid, transitions by means of higher multipoles may be neglected. Indeed, early experiments showed good agreement with theoretical predictions(1).

At increased photon energies the theoretical problem is more complex. As the dipole approximation becomes less valid it is necessary to take into account higher multipole moments. In order to do this the deuteron wave function and exchange current phenomena must be quantitatively understood. Measurements between 50 mev and the meson threshold (2,3,4) yielded larger cross sections than would be indicated by reasonable assumptions concerning the potential and exchange currents (5,6). It was therefore hypothesized that even below the meson threshold photodisintegration takes place partly through the production and absorption of virtual mesons with the result that mesonic effects would have to be considered explicitly

and not only in the sense that they determined the deuteron wave function.

The appearance of a resonance in the elastic photodisintegration* cross section at 250 mev (3,4) led to Zachariasen's calculation (7) which maintained that the largest contributions to the matrix elements were due to terms involving the scattering and absorption of photoproduced mesons. The qualitative agreement of this calculation with experiment is a confirmation of the idea that mesons play a direct role since computations (5,6) which failed to take account of them predicted nonresonant behavior as well as much smaller cross section values. It would seem that as the photon energy is further increased, meson terms would continue to dominate the matrix elements. The theoretical problem thus becomes one of considering meson production, scattering, and absorption in a system composed of two almost free nucleons whose separation is given by the deuteron wave function.

In principle high energy elastic photodisintegration experiments in conjunction with meson theory should yield the shape of the deuteron potential. However, it appears that a more developed meson theory would by itself solve the problem of the deuteron wave function and the value of elastic photodisintegration experiments is in providing a consistency test for theories of strong interactions rather than in giving direct insight into such phenomena.

---

* Elastic photodisintergration implies the reaction $\gamma + D \rightarrow P + N$

From the experimental point of view, neglecting the problems associated with obtaining and maintaining a photon source, the measurements are made in a straightforward manner between the thresholds for photodisintegration and meson production. At energies above the meson threshold the experimental difficulties increase greatly. The cross section becomes small both absolutely and in comparison with that for the various competing processes. In addition there are nontrivial difficulties associated with detecting the high energy protons emitted in the photodisintegration reaction.

The present experiment was done in order to examine the behavior of the cross section for the reaction $\gamma + D \rightarrow P + N$ for photon energies between 500 and 900 mev. Protons from the reaction were detected with a counter telescope. The measurements were a continuation of those made in this laboratory by Keck and Tollestrup (4). An excitation curve was measured at 90° in the laboratory and center of mass angular distributions were obtained at laboratory photon energies of 500 and 700 mev. The amount of data that could be taken was limited by low cross sections and difficulties inherent to counter telescopes at high energies. The excitation curve agreed fairly well with that of the previous experiment in the overlapping region. The differential cross section decreased from 1.4 μb/steradian at 433 mev to less than 0.05 μb/steradian at 900 mev. These results do not contradict any qualitative arguments which might be made about the elastic photodisintegration process in this energy region.

II

EXPERIMENTAL PROCEDURE

A. General Considerations

The elastic photodisintegration of the deuteron implies the reaction

$$\gamma + D \rightarrow P + N \qquad (1)$$

as distinguished from inelastic photodisintegration

$$\gamma + D \rightarrow Y_i + Y_i + X \qquad (2)$$

where Y_i is either a proton or a neutron and X stands for other reaction products.

Measurements of the elastic photodisintegration cross section are made by observing the protons arising from reaction 1. If the proton energy and angle are determined by the experimental apparatus, two-body kinematics fix the energy of the photon which causes the reaction. However, knowledge of the proton energy and angle is not sufficient to rule out the possibility that some of the observed protons originated in a reaction of type 2.

It is shown in Appendix I that for a given proton vector momentum the minimum photon energy which can cause an inelastic photodisintegration is greater than that causing the elastic process, and that the minimum photon energy is required when all reaction products except the proton being observed have the same vector velocity. One set of curves in figure 1 shows that nucleon kinematics for process 1. A second set refers to the nucleon kinematics at the minimum photon energy required for single pion production from deuterium. (The

Figure 1

Proton energy versus proton angle at different photon energies for the reactions:

a. $\gamma + D \rightarrow P + N$

b.* $\gamma + D \rightarrow P + (N + \pi^o)$

c. $\gamma + P \rightarrow P + \pi^o$

---

* In this case neutron and pion are at rest with respect to each other.

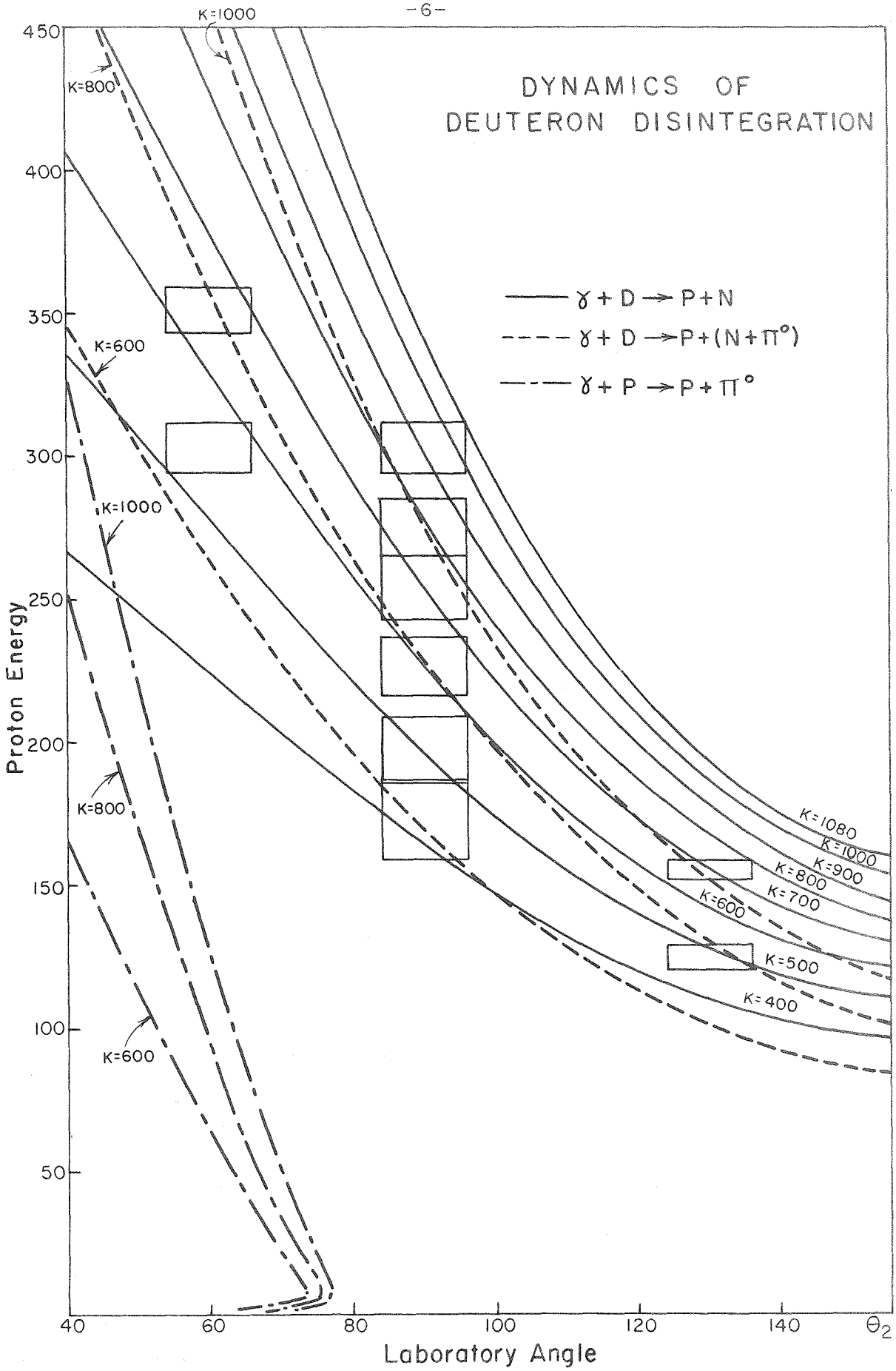
DYNAMICS OF
DEUTERON DISINTEGRATION
γ + D → P + N
γ + D → P + (N + π°)
γ + P → P + π°
K=1000
K=800
K=600
K=1000
K=800
K=600
K=1080
K=1000
K=900
K=800
K=700
K=600
K=500
K=400
Proton Energy
Laboratory Angle
θ2
450
400
350
300
250
200
150
100
50
40
60
80
100
120
140

reaction $\gamma + D \rightarrow P + N + \gamma'$ has a lower threshold but its cross section is very small.) Single pion production has the largest cross section in the energy range of this experiment and is expected to be the only process from which nonelastic protons might be detected.

There are photons of all energies between zero and a maximum E_o in the bremsstrahlung beam but the sharp cutoff of the spectrum makes it possible to insure the exclusion of processes like 2 by setting the end point below where it is possible to detect protons from inelastic reactions but sufficiently high so that elastic protons are counted. In general it was possible to select an end point which fulfilled these conditions. However, at some places where data was taken, lowering the upper limit of the photon spectrum to eliminate protons from inelastic reactions would cut into the photon energy interval which corresponded to the finite energy and angular acceptance of the detector. In such a case the maximum energy of the bremsstrahlung was still set slightly higher than the maximum photon energy producing elastic protons accepted by the detector. This was done at the expense of making it possible for inelastic protons to be counted. Contributions from inelastic processes were found by measuring the yield per equivalent quantum* as a function of end point energy. The elastic yield should be independent of the end point as

---

* An equivalent quantum is that amount of bremsstrahlung energy which is equal to the total energy of the electron producing the bremsstrahlung. This is a convenient quantity since the bremsstrahlung spectrum from an ideal thin target is such that in each equivalent quantum the number of photons of energy k in energy interval dk is approximately constant regardless of end point energy as long as k is below the end point.

long as the bremsstrahlung spectrum contained all photon energies which could produce elastic protons in the angular and energy range defined by the detector while the yield from inelastic reactions should increase as the maximum photon energy is raised. This method was able to demonstrate that the inelastic contribution was nearly negligible (see data analysis).

There are several experimental methods which might be used to count protons. The most positive way of identifying them and gaining a maximum of information from each event is through the use of a deuterium cloud chamber in a strong magnetic field. The Cornell experiment on multiple meson photoproduction (8) in a hydrogen diffusion cloud chamber indicates that a measurement with 20% statistics would need on the order of one million pictures. About 1% of these would require analysis in addition to scanning.

A second method of detecting protons is based on the use of a magnet for momentum analysis in conjunction with scintillation and Cerenkov counters for velocity determination. A magnet system subtending a solid angle of 0.015 steradians and having a $\Delta P/P$ of 0.1 is desirable because of the low cross section. At high proton energies where differences in specific ionization are too small to be useful, electrons and pions might be eliminated by Cerenkov counters having a threshold at $\beta = 0.8$ and an efficiency of greater than 99%. If static field magnets were employed the necessarily long particle trajectories could be used in measuring velocity by the time of flight technique.

The counter telescope* may also be used to detect protons. This device has the advantages of subtending relatively large solid angles, being easy to change from one mean energy and angle setting to another, and requiring little physical space. On the other hand as the energy of the observed particle increases, the usefulness of the telescope rapidly diminishes. The maximum proton energies for which proton telescopes are useful varies from about 300 to 500 mev depending on the proton flux relative to that of other particles.

The biggest problem results from having to insert sufficient absorber material in the telescope to stop the particle. The use of telescopes is based on the assumption that a charged particle loses energy only by transferring its energy to atomic electrons. With particles which undergo nuclear interactions this is a good approximation only for small amounts of absorber. As the energy of the particle increases and more material is required to stop it, the probability of a nuclear interaction becomes appreciable. In this case a large fraction or indeed all of the kinetic energy is dissipated in one collision. (Seventy-five mev protons have about a 93% probability of losing all their energy in copper by ionization alone. This probability is decreased to 50% for 300 mev protons.)

A result of nuclear interactions is that a certain fraction of the protons that would ordinarily be counted are lost. Also some that initially had sufficient range to reach the veto counter lose a large amount of energy in the absorber, stop in ΔR and are counted.

---

* Telescope principles are discussed in section E of Experimental Procedure.

It is also possible that nuclear stars caused by either pions or protons emit secondary particles with the net result that the telescope cannot distinguish between this sequence of events and a photodisintegration proton of the proper energy. The exact contribution of these effects to the counting rate is difficult to determine so that uncertainties of order of magnitude of those in the absorption cross sections (about 10% at 300 mev) are introduced.

It is not possible to eliminate some of the effects of nuclear interactions by pulse height analysis performed on pulses which are made before very much absorber is traversed since for high energies the particles must be slowed down before mass separation through difference in specific ionization is feasible. In practice due to poor light collection properties, statistical fluctuations in energy loss, photocathode inefficiency, and the large ratio of pions to protons, a proton has to have a specific ionization of at least one and one half times that of minimum ionizing particles before it can be distinguished from such particles.

The single counting rates in telescope counters are much higher than are those in counters used with a magnet. Thus the electronics used in conjunction with a telescope must be faster than those generally employed in the magnet technique. At the time when this experiment was performed fast electronics implied greater overall complexity but new developments promise that this disadvantage is only a temporary one.

In comparing the various methods of proton detection it is seen that the cloud chamber is superior to the magnet in that more

information is obtained concerning individual events. However, the large number of pictures which is required makes the magnet method more feasible than the cloud chamber. Since at high energies the magnet suffers from deficiencies which can be remedied rather than inherent limitations, it is better than the counter telescope from the point of view of obtaining accurate data for a large number of points. But the construction of a system of pulsed or fixed field bending and focusing magnets and the associated counters would require a considerable expenditure of time and funds.

For the experiment described here the counter telescope was chosen as a compromise between clarity of results and expenditure of resources and effort. With the above shortcomings in mind it was decided to take data at the points designated by the boxes in figure 1. The manner in which the limitations were taken into account is described in following sections.

B. Photon Beam

The photon source was the bremsstrahlung beam generated by the Cal Tech snychrotron. The beam was emitted in 20 millisecond bursts at a repetition rate of approximately one pulse per second and during emission the intensity was constant to within 20%. The beam had an energy distribution which was nearly that characteristic of bremsstrahlung produced in a thin target. The end point energy, E_o, could be continuously changed from 550 to 1080 mev.

Useful data was obtained with intensities ranging from 10^7 to $2 \cdot 10^8$ equivalent quanta per pulse.

An air filled, thick walled ion chamber was used to monitor the beam (9). In order to make an absolute measurement of the energy in the beam this ion chamber was calibrated against one designed by Wilson (10). Knowing the shape of the bremsstrahlung spectrum and the amount of energy in the beam, it was possible to calculate N(k)dk, the number of photons of energy k in energy interval dk, which passed through the deuterium target.

C. Target

Liquid deuterium was contained in the same apparatus as that used for hydrogen in other Cal Tech synchrotron experiments (11). Since the system had been designed for use with either hydrogen or deuterium no fundamental changes were required for this experiment. An effective length of 7.24 cm and a nominal deuterium density of 0.1693 gm/cm^2 were used for the target parameters. Spectroscopic analysis showed that the deuterium was contaminated by an amount of H_2 and HD (12) so that the actual deuterium density varied from 98.6% to 97% of the above value during the course of the experiment. Other contaminants were not important since these crystallized and sank to the bottom of the deuterium container where they were below the lower boundary of the beam. Particles produced in the center of the target passed through 0.65 gm/cm^2 of deuterium and radiation shields and mylar walls consisting of 0.007 gm/cm^2 aluminum, 0.068 gm/cm^2 copper, 0.043 gm/cm^2 oxygen, and 0.081 gm/cm^2 carbon.

D. Telescope Table

The telescope table was constructed in such a way that telescope and magnet experiments could be done simultaneously. This involved permitting the table top to rotate about an axis which was fastened to the magnet and clamping one point of the edge of the table top to a fixed post. The axis was supposed to be coaxial with the magnet pivot so that when the magnet angle was varied the orientation of the table top with respect to the laboratory would not change. In reality, however, the magnet pivot and table axis were not coaxial with the result that changes of the magnet angle produced a displacement of the table axis. Since the pivot for the telescope cart and the table axis had the same center the solid angle subtended by the telescope was a function of the position of the table axis and hence of the magnet angle. This function was measured and solid angle corrections were made to the data. The solid angle variation had a maximum of 5% and averaged 2%.

E. Telescope and Electronics

The mass and energy of a moving charged particle can be determined from measurements of the particle's range in an absorbing medium and its rate of energy loss, dE/dx, at some point in the medium. In principle the information may be obtained with a telescope* consisting of only three counters, where one measures dE/dx and the other two define the range. For this experiment, two dE/dx counters

* In their theses, Worlock (11) and Ernstene (13) present additional details concerning the theory and operation of counter telescopes.

and a Cerenkov counter to veto fast particles were added in order to differentiate more clearly between protons and the much more abundant pions and shower products. The probability that the latter appear to be protons by spuriously producing the proper combination of pulses was greatly reduced with the addition of the other counters.

Figure 2 is a plan view of the experiment and figure 3 shows details of the 6 counter telescope. Counters #1, #3, #4, #5, and #6 were plastic scintillators whose light output was proportional to the amount of energy lost by particles in traversing them. C was a Cerenkov counter made out of UVT lucite. This type of lucite has higher transmission in the ultraviolet region and scintillates less than the more common UVA lucite. Counter dimensions are given in table I. The telescope was mounted on a movable cart which made it possible to change the angle between telescope axis and bremsstrahlung beam. Proton energy was determined by the total amount of material the particle had to traverse between the point of production and the point where it stopped. This energy was varied by using the different absorbers listed in table II.

Counters #1, #3, #4, and #5 were placed in coincidence while C and #6 were in anticoincidence. The coincidence-anticoincidence combination of #5 and #6 indicated that particles traversing the telescope had come to rest in either #5 or absorber E. Counters #1, #3, and #4 measured dE/dx of the particles passing through them. The Cerenkov counter detected $\beta = 1$ particles with an efficiency of about 95%. A particle was called a proton if it made no Cerenkov

Figure 2

Plane view of experiment.

Scale is 1 cm $\sim$ 4 inches.

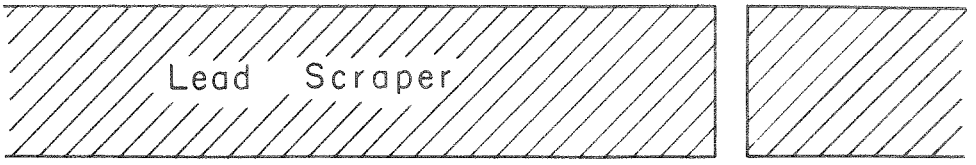
Lead Scraper

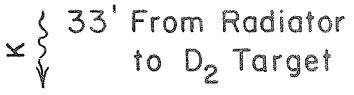
33' From Radiator
to D_2 Target

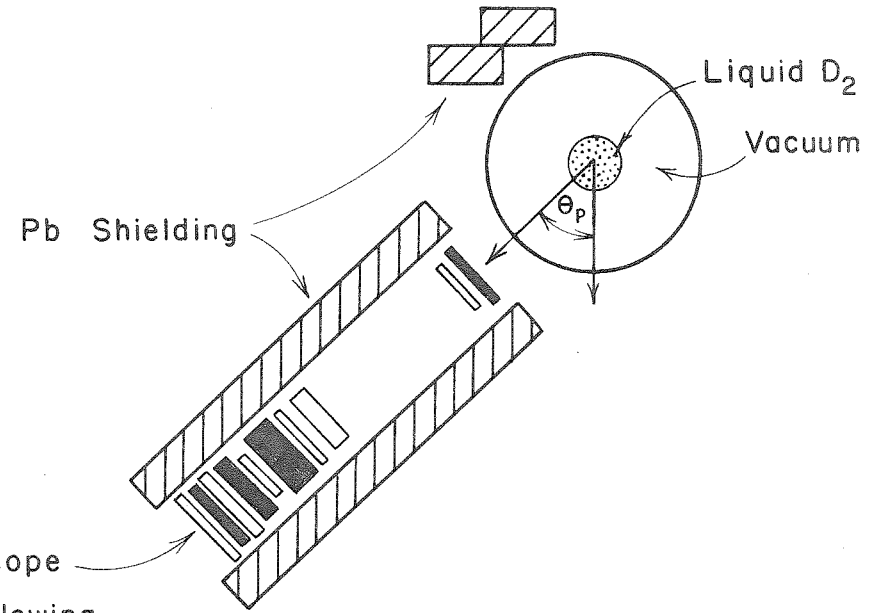
Liquid D_2
Vacuum
θ_p
Pb Shielding
Telescope
(See Following
Figure For
Details)
30' From D_2
Target to
Ion Chamber
Scale: 1cm = 4"
Ion Chamber

Figure 3

Plan view of counter telescope (schematic).

Scale is 0.5 of full size. A, B*, B, C, D, and E are absorbers. #1, #3, #4, #5, and #6 are plastic scintillation counters. C is a lucite Cerenkov counter. Protons travel in direction of arrow.

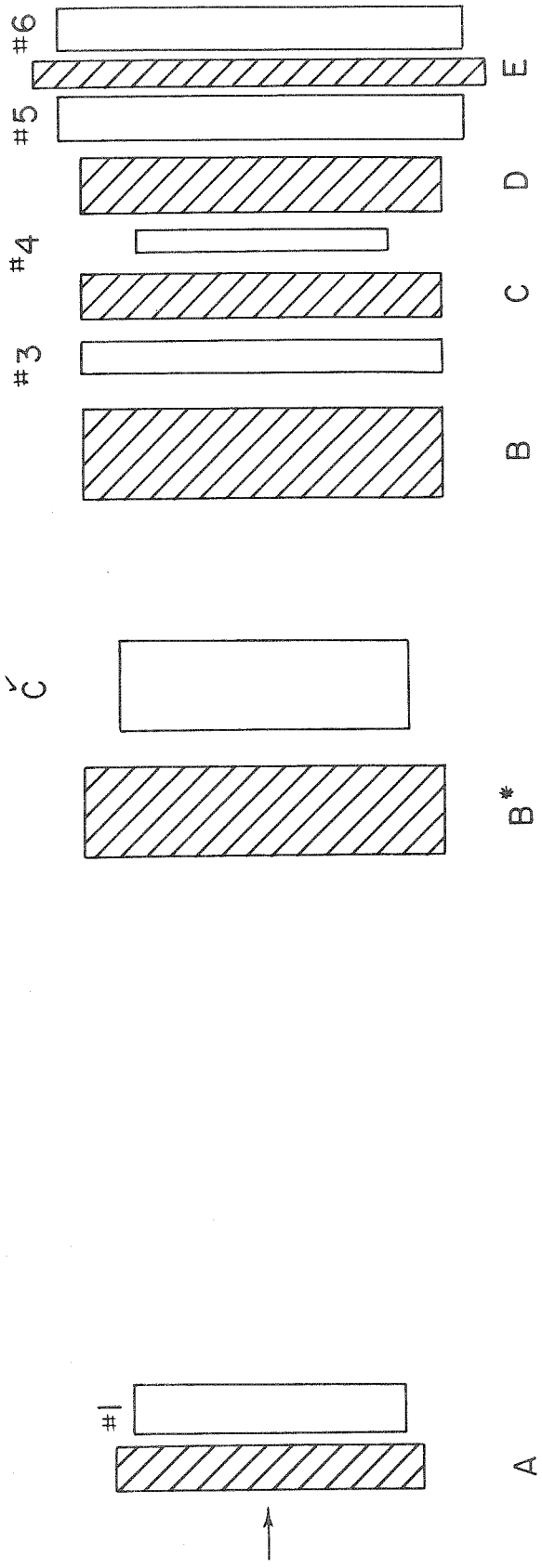
#6
E
#5
D
#4
C
#3
B
C
B*
#1
A

Table I

Counter No.	Dimensions	Material
1	3.25" X 2.25" X 0.490"	plastic scintillator
2	6" X 4" X 0.787"	" "
C	3.75" X 3.19" X 0.995"	UVT lucite
4	3.39" X 2.75" X 0.243"	plastic scintillator
5	6.50" X 4.50" X 0.490"	" "
6	6.50" X 4.50" X 0.490"	" "

Table II

Column 1: Point number (see Table III).

Column 2: Mean proton range, gm/cm^2 of copper*.

Column 3: Absorber A, gm/cm^2 of CH_2.

Column 4 - 7: Absorbers B - E, gm/cm^2 of copper.

Column 8: ΔR, gm/cm^2 of copper.

Point No.	R	A	B(B')	C	D	E	ΔR
1	30.3	0.83	0	0	16.20	5.65	7.65
2	38.0	0.83	0	6.56	16.20	5.65	7.65
3	48.0	1.27	3.94	12.10	16.20	5.65	7.65
4	58.7	1.27	15.35	12.10	16.20	5.65	7.65
5	66.3	1.27	22.80	12.10	16.20	6.65	7.65
6	78.0	1.27	36.10	12.10	16.20	5.65	7.65
7	66.3	1.27	22.80	12.10	16.20	5.65	7.65
8	98.5	1.27	32.26**	24.82	33.03	5.65	7.65
9	18.4	0.83	3.24	0	2.81	0	1.31
10	26.0	0.83	10.63	0	2.81	0	1.31

* Includes average loss in target material.

** At all points except No. 8 absorber B' was zero. At No. 8 B' had the above value and B was zero.

light, stopped in #5 or E, and lost the proper amount of energy in the dE/dx counters.

Biases were set on the signals from counters #1, #3, and #4 so that the discriminators corresponding to these counters would be triggered only by pulses which were as large as those expected from protons. Proton energy was in an interval between E and $E + \Delta E$ corresponding to a range interval between R and $R + \Delta R$. Using the technique of Keck and Tollestrup (4) which consists of measuring the proton counting rate as a function of ΔR and then extrapolating to zero counting rate, it was shown that ΔR was equal to counter #5 plus absorber E with an uncertainty of $\pm$ 0.15 gm/cm^2 of copper.

The gain of the Cerenkov counter was set as high as possible but below the point where the scintillations in the lucite due to relatively highly ionizing protons would cause such protons to be rejected. Effects of scintillation were measured by placing the Cerenkov counter in coincidence with the rest of the telescope. With protons which were as highly ionizing as any observed in the experiment the proton counting rate was measured as a function of the Cerenkov counter high voltage.

Although biases were set on the dE/dx counters so that their discriminators would trigger only on proton size pulses, it was possible for pions with low specific ionization to trigger the discriminator by giving rise to a pulse as large as that expected from protons (Landau effect). For a particle to be recorded as a proton it was necessary that proton size pulses occur in all three dE/dx counters. Since the occurrence of big pulses is a statistical

effect and was therefore uncorrelated among the various dE/dx counters, the use of three detectors to measure dE/dx greatly reduced the number of counts due to this effect.

In the telescope pions might give rise to interactions in which energetic protons were produced. Any counter in the telescope that was placed beyond the point where the proton was formed could not distinguish pion produced protons from protons produced at the target. The effect was minimized by placing most of the absorber after the first dE/dx and Cerenkov counters so that fast pions would have to produce protons in or before absorber A. For slow or stopping pions which might make a big pulse in #1 and no Cerenkov pulse there was in general not sufficient energy available to make a proton which could get as far as counter #5.

The efficiency of the telescope in discriminating against the above effects, as well as those due to protons suffering nuclear collisions in the absorber, was observed by several methods.

Since the statistical fluctuations in pulse height were uncorrelated, the existence of a proton peak in #1 indicated that a negligible number of counts were due to this phenomenon.

A lead converter placed in front of absorber A demonstrated that there were no counts due to showers from pion γ-rays.

It was possible to set the telescope in configurations where kinematics forbade the presence of protons other than those which might be made in the walls of the target. With deuterium in the target, kinematically forbidden regions were reached by moving the telescope to more backward angles, increasing the amount of

absorber so that higher energy protons were required, or by lowering the end point of the bremsstrahlung spectrum. With hydrogen in the target, no real counts should have been observed when the telescope was set at an angle and energy to detect protons from photodisintegration. Hydrogen runs were made with relatively large amounts of absorber in the telescope (T_p = 278 mev, θ = 90°; T_p = 354 mev, θ = 60°) to observe the effect of fast pions and with the minimum amount (T_p = 130 mev, θ = 130°) where difficulties might be expected from slow pions. Except at θ = 60°, T_p = 354 mev with H_2 in the target, all runs in kinematically forbidden regions gave rates which were equal within statistics to the empty target rates.

For the point corresponding to a proton angle of 60° and a photon energy of 700 mev there were counts from hydrogen under the proton peak which could not be ascribed to the target walls. At this point counter #1 was not useful since the protons and pion peaks overlapped. It was also necessary to place 1 inch of copper absorber in front of the Cerenkov counter so that at this point in the telescope protons destined to stop in absorber E would have had their energy degraded to below 320 mev, the threshold for protons to make Cerenkov light in lucite. Thus before the telescope could differentiate between pions and protons there was a non-negligible amount of absorber in which pions might interact and produce fast secondary protons. The contribution from pions produced in hydrogen was measured and, after normalization to deuterium, added to the empty target background.

A block diagram of the electronics is shown in figure 4. The resolving time of each circuit is shown in the pertinent block. The phototubes were RCA 6810's and 6810A's. From counters #3 and #4 signals were taken from both dynode #12 and the anode. The anode signals were used to run the fast coincidence circuits. After amplification, gating, and further amplification, the dynode #12 signals from #3 or #4, or the anode signals from #1 or #5, could be pulse height analyzed. Placing the Cerenkov counter in coincidence with #3 and then using the C + #3 coincidence signal as a veto in the (1 + 4 + 5)-6-(2 + 3) circuit allowed monitoring of the Cerenkov counting rate.

F. Data Collection

The number of points at which data might be taken was limited by the low cross section and the inherent deficiencies of telescopes at high proton energies. Measurements were made at the points specified by the boxes in figure 1 and in table III. After the telescope was aligned data was collected during a four month period. The alignment procedure and data taking required roughly $3 \cdot 10^{14}$ equivalent quanta.

The equipment was periodically calibrated using a carbon target with the telescope set in a standard position with a standard amount of absorber. In this configuration the position of the proton peaks in counters #1, #3, and #4 was checked. With biases in counters #3 and #4 set so that the pulse height analyzer would be triggered only by protons stopping in #5 or absorber E, the pulse height distribution in #5 was examined. These pulse height distributions were sensitive to changes in gain of the photomultipliers,

Figure 4

Electronic block diagram.

Power supplies are omitted. In the block corresponding to each coincidence circuit the resolving time of the circuit is given. The symbols have the following meaning:

G - Fast Gate, Model 15, gate length 0.1 μs

A - Amplifier, Model 552, maximum gain 2500; rise time 0.7 μs

D - Discriminator, Model #1

HPA - Hewlett Packard Distributed Amplifier, maximum gain 20 db, rise time 2.6 mμs

HPB - Hewlett Packard Distributed Amplifier, maximum gain 15 db, rise time 2.6 mμs

T - Attenuation network

All phototube signals were taken from the anode unless otherwise specified. Dy #12 and Dy #14 mean signals were taken from these dynodes. Anode signals were negative. Dy #12 and Dy #14 signals were positive.

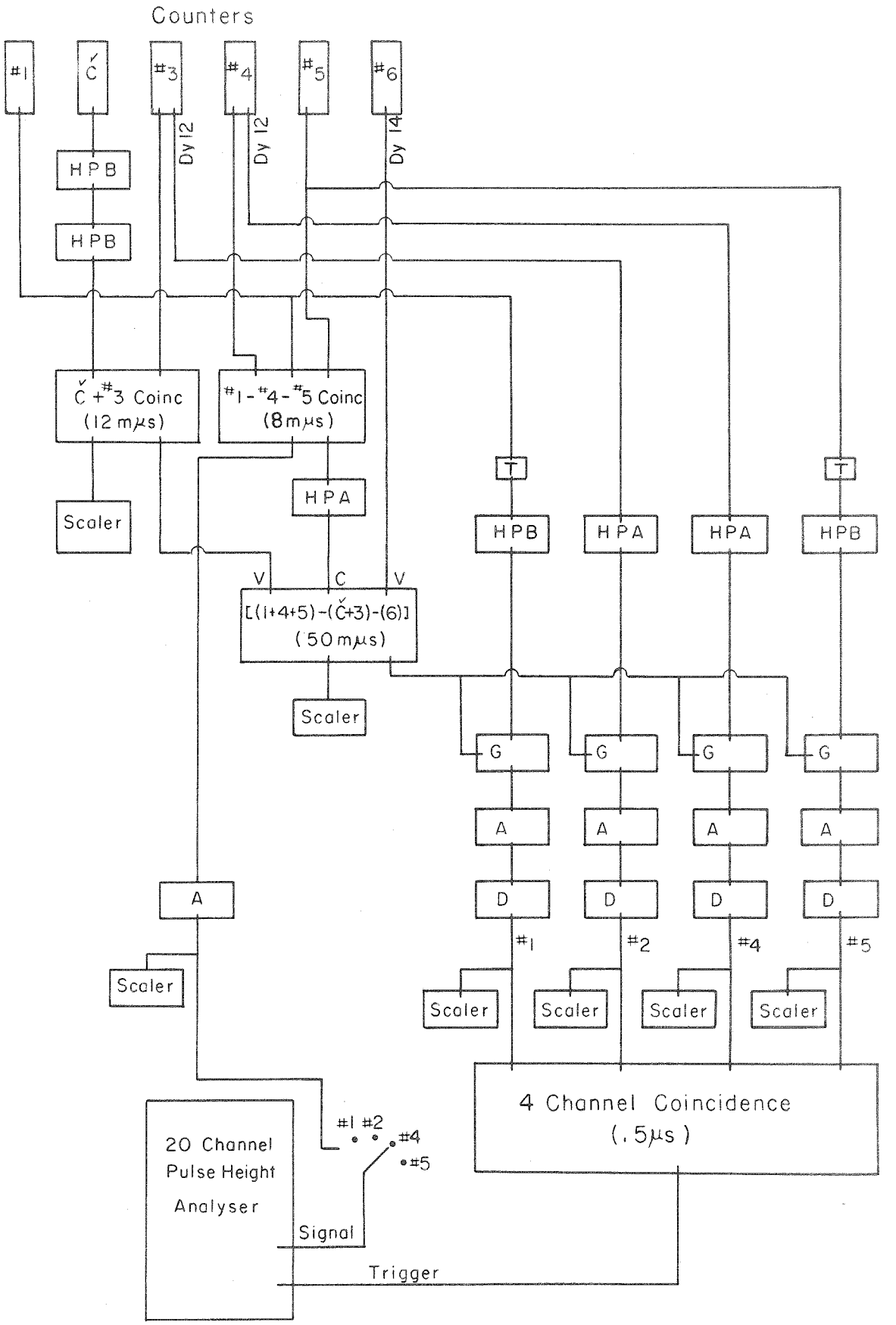
Counters
#1
Č
#3
#4
#5
#6
Dy 12
Dy 12
Dy 14
HPB
HPB
Č+#3 Coinc
(12 mμs)
#1-#4-#5 Coinc
(8mμs)
Scaler
HPA
T
T
HPB
HPA
HPA
HPB
V
C
V
[(1+4+5)-(Č+3)-(6)]
(50 mμs)
Scaler
G
G
G
G
A
A
A
A
A
D
D
D
D
#1
#2
#4
#5
Scaler
Scaler
Scaler
Scaler
Scaler
4 Channel Coincidence
(.5μs)
20 Channel
Pulse Height
Analyser
#1 #2
#4
#5
Signal
Trigger

Table III

Column 1: Point number

Column 2: Mean photon energy, mev

Column 3: Mean proton energy, mev

Column 4: Mean proton laboratory angle, degrees

Column 5: Mean proton c.m. angle, degrees

Column 6: End point energy at which reduced data was obtained

Point No.	k	T_p	θ_{lab}	θ_{cm}	E_o
1	438	177	90	109	600
2	513	201	90	111	700
3	614	230	90	113	800
4	716	258	90	114	900
5	793	278	90	116	1000
6	913	306	90	118	1080
7	503	278	60	80	600
8	646	354	60	82	900
9	510	130	130	145	600
10	734	160	130	148	900

gates and amplifiers. If the number of protons per equivalent quantum did not change from one calibration run to the next, it was assumed that the overall efficiency of the telescope had not changed. A display of those output pulses from the 1 + 4 + 5 coincidence circuit which corresponded to protons traversing the telescope provided a simple check on the timing of counters #1, #4, and #5 with respect to each other.

For each point the deuterium and empty target data was collected in periods separated by time intervals of one week or more. The monitors provided a check on the internal consistency of the counting rates at a given point. Pulse height distributions from deuterium, having the same general shape as those from carbon, were another indication that the equipment was in working order. Typical pulse height distributions from deuterium and carbon are shown in figure 5.

Runs were made with hydrogen, deuterium and an empty target. At all the points except the one for which there was a contribution from hydrogen the ratio of the length of running time with deuterium to that with an empty target was approximately equal to the square root of the ratio of the respective counting rates. For a given length of running time this division between empty and full target minimizes the statistical error.

Figure 5

Typical proton peaks in counter #1 from deuterium and carbon.

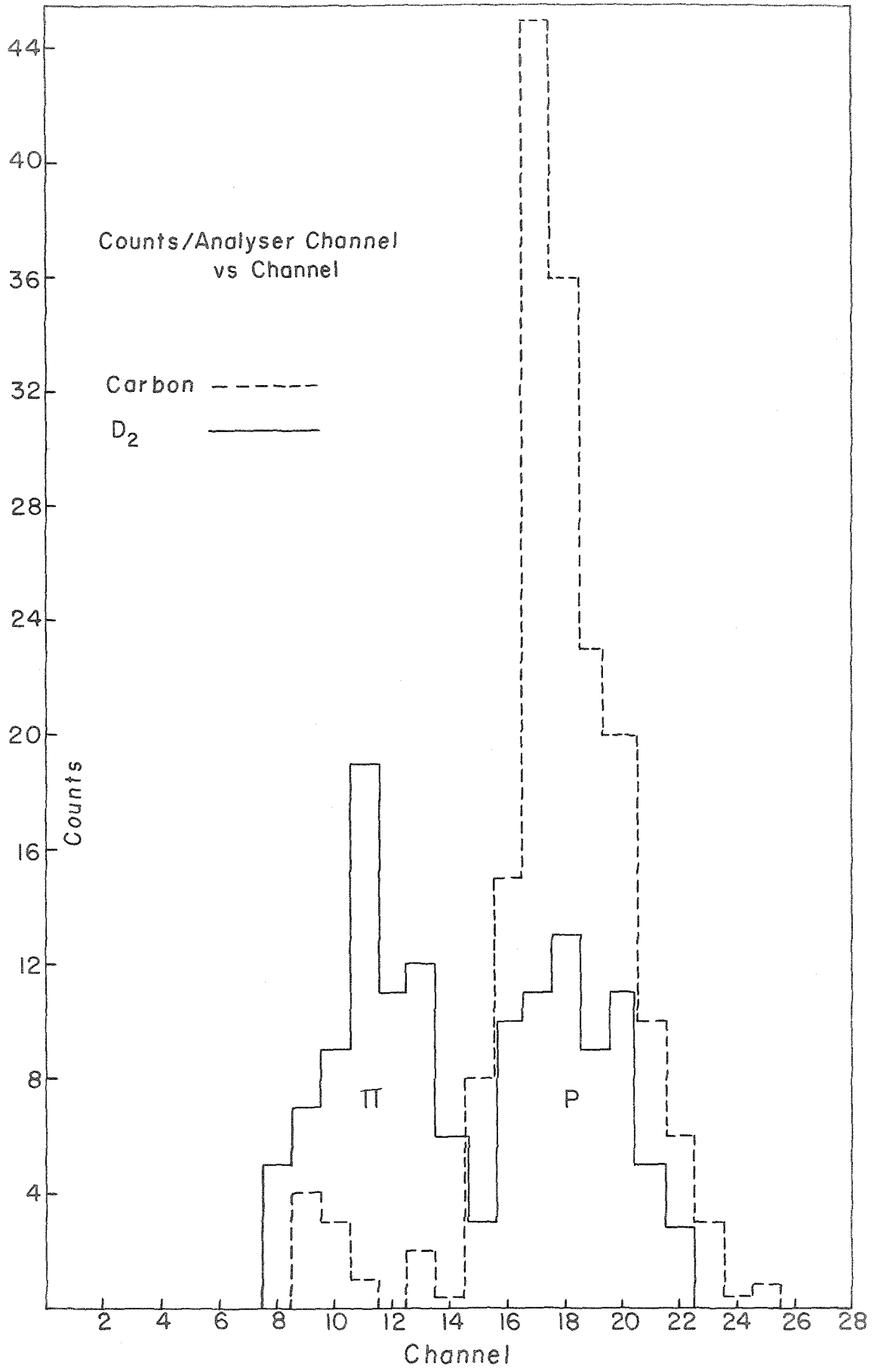
Counts/Analyser Channel
vs Channel
Carbon
D_2
Counts
Channel
π
P
44
40
36
32
28
24
20
16
12
8
4
2
4
6
8
10
12
14
16
18
20
22
24
26
28

III

DATA REDUCTION

Data was obtained in the form of a certain number of counts per B.I.P.* of bremsstrahlung beam. The observed counting rate was corrected for backgrounds and nuclear interactions in the telescope in order to obtain a corrected rate which is related by measurable quantities to the center of mass differential cross section. Thus

$$C.R. = N_T \frac{1{\cdot}20{\cdot}10^{12} R(E_o) B(E_o,k)}{E_o k} \frac{dk}{dT} \frac{dT}{dR} \, dR \, \frac{d\Omega'}{d\Omega} \frac{d\sigma}{d\Omega'} d\Omega \qquad (3)$$

where C.R. = corrected number of protons detected per B.I.P.

N_T = number of target nuclei per square centimeter

$1{\cdot}20{\cdot}10^{12} \frac{R(E_o)B(E_o k)}{E_o k} \, dk/dT \, dT/dR \, dR$ = number of photons per B.I.P. with energy k in energy interval dk, which can produce elastic photodisintegration protons of energy T in energy interval dT where dR is the telescope range interval corresponding to dT. $B(E_o,k)/k$ is the bremsstrahlung spectrum as measured by Emery, Donoho, and Walker. $R(E_o)$ takes into account the fact that the number of ions produced in the ion chamber per unit of beam energy has a slight dependence on the end point energy of the bremsstrahlung spectrum. Values for $R(E_o)$ and $B(E_o,k)$ are given in table IV.

---

* B.I.P. means Beam Integrator Pulse. One B.I.P. is $1{\cdot}20\ 10^{12}$ $R(E_o)$ mev of energy in the bremsstrahlung beam. $R(E_o)$ is of the order of unity and is discussed elsewhere in this section.

Table IV

For a set of values of E_o and k table IV gives the magnitude of the functions $B(E_o,k)$ and $R(E_o)$ which are discussed on the preceding page.

	E_o						
	550	600	700	800	900	1000	1080
400	0.90	0.90	0.91	0.93	0.93	0.95	0.98
500	0.90	0.90	0.90	0.90	0.91	0.93	0.94
600	0.90	0.90	0.90	0.90	0.90	0.90	0.91
k 700	0.90	0.90	0.90	0.90	0.90	0.90	0.90
800	0.90	0.90	0.90	0.90	0.90	0.90	0.90
900	0.90	0.90	0.90	0.90	0.90	0.90	0.90
	0.89	0.91	0.94	0.98	1.02	1.05	1.08
	$R(E_o)$						

$B(E_o,k)$

$d\Omega'/d\Omega$ = solid angle transformation between center of mass and laboratory

$d\sigma/d\Omega'$ = center of mass differential cross section

$d\Omega$ = laboratory solid angle

The following procedure was employed in obtaining the corrected proton counting rate from the observed rate.

A) Observed proton rates

For each run the number of counts under the proton peak was summed. An error of $\pm$ 5% was ascribed to uncertainties in the summation process.

B) Backgrounds

The empty target rates were subtracted from those obtained in the deuterium runs. The former lay between 10% and 50% of the latter. At $\theta = 60^{o}$, $T_p = 354$ mev, twice the hydrogen contribution was subtracted from the deuterium rate. This method of subtraction assumed the hydrogen contribution to be due to charged pions. An average π^-/π^+ ratio of 1.0 at this angle implied that there should be twice as many pions per nucleus from deuterium as from hydrogen.

C) Absorption

The largest correction to the data was for the inelastic interaction of protons in the copper absorber. An absorption measurement made at Berkley by Richardson et al. (14) provided the basis for this correction. The mean discrepancy between the absorption correction used here and those used by other authors* varies

---

* Worlock (11) used a correction obtained from a theoretical computation. Chamberlain et al. (15) measured an integral absorption curve similar to that of Richardson (14).

between 2% for 127 mev protons and 10% for 354 mev protons. An absorption error equal to the mean discrepancy was assigned.

D) Scattering

Computations showed that less than 1% of the protons were lost due to large angle scattering processes except at $\theta = 60^{\circ}$, $T_p = 354$ mev. Here the loss was found to be about 1.5%. An error of 1% is added due to uncertainties in the large angle scattering calculations. Inefficiencies introduced by multiple coulomb scattering were calculated and found to be insignificant.

E) Degraded protons

The end point of the bremsstrahlung spectrum was usually several hundred mev above the median photon energy which produced protons stopping in the telescope. An effect might be expected from protons, initially of a higher energy than the telescope acceptance, which suffer inelastic interactions in the absorber. An increase in the end point energy did not show a statistically significant increase in the cross section. Table V shows the number of counts per equivalent quantum as a function of end point energy for each point. This result implies that most protons lose an appreciable amount of their energy when they have an inelastic collision. An assymetric error equal to minus one half of a statistical deviation in the deuterium minus empty target counting rate was assigned to compensate for uncertainties introduced by this effect.

The conversion from counting rate to C.M. differential cross section was obtained by substituting corrected counting rates and other measured parameters in the above relation (equation 3).

Table V

Column 1: Point number

Column 2: End point energy

Column 3: Full target counting rate; "protons" per B.I.P.

Column 4: Background counting rate; "protons" per B.I.P.

Column 5: Deuterium counting rate; protons per 10^{10} equivalent quanta.

Point No.	E_o	$(C.R.)_{F.T.}$	$(C.R.)_{bkg}$	$(C.R.)_{D_2}$
1	550	1.64 ± 0.15	$0.20 \pm 0.03^*$	8.23 ± 0.86
	600	1.58 ± 0.14	0.20 ± 0.04	8.41 ± 0.91
	800	1.63 ± 0.05	$0.24 \pm 0.03^*$	10.17 ± 0.44
	1080	1.63 ± 0.08	$0.28 \pm 0.03^*$	11.48 ± 0.76
2	600	0.62 ± 0.04	$0.12 \pm 0.03^*$	3.05 ± 0.31
	700	0.71 ± 0.06	0.12 ± 0.02	3.98 ± 0.41
	800	0.72 ± 0.04	$0.12 \pm 0.03^*$	4.53 ± 0.38
	1000	0.73 ± 0.03	$0.12 \pm 0.03^*$	4.91 ± 0.32
3	700	0.28 ± 0.03	$0.034 \pm 0.008^*$	1.71 ± 0.21
	800	0.33 ± 0.05	0.034 ± 0.010	2.26 ± 0.38
	900	0.38 ± 0.04	0.027 ± 0.015	2.86 ± 0.33
	1000	0.36 ± 0.05	$0.034 \pm 0.008^*$	2.91 ± 0.44
4	600[i]	0.005 ± 0.005		0.034 ± 0.034
	900	0.127 ± 0.018	0.025 ± 0.009	0.832 ± 0.163
	1000	0.121 ± 0.014	0.035 ± 0.009	0.758 ± 0.150
	1080	0.091 ± 0.017	$0.040 \pm 0.010^*$	0.466 ± 0.180
5	700[i,iii]	0.012 ± 0.007	$0.011 \pm 0.005^*$	0.007 ± 0.085
	900[iii]	0.072 ± 0.019	$0.011 \pm 0.005^*$	0.514 ± 0.163
	1000	0.061 ± 0.010	0.011 ± 0.006	0.441 ± 0.106
	1080	0.061 ± 0.005	0.011 ± 0.004	0.457 ± 0.055
6	1080	0.026 ± 0.006	0.010 ± 0.004	0.147 ± 0.064
7	600	0.396 ± 0.033	0.064 ± 0.014	2.02 ± 0.22
	700	0.397 ± 0.015	0.095 ± 0.016	2.07 ± 0.14
	800	0.415 ± 0.022	0.077 ± 0.014	2.55 ± 0.19
	900	0.410 ± 0.029	0.086 ± 0.013	2.61 ± 0.26
	1000	0.494 ± 0.018	0.094 ± 0.012	3.44 ± 0.19
	1080	0.521 ± 0.056	0.090 ± 0.010	3.81 ± 0.50

Table V
(continued)

Point No.	E_o	$(C.R.)_{F.T.}$	$(C.R.)_{bkg}$	$(C.R.)_{D_2}$
8	800	0.097 ± 0.008	$0.024 \pm 0.012^{*iv}$	0.55 ± 0.10
	850	0.094 ± 0.013	$0.030 \pm 0.012^{*iv}$	0.50 ± 0.14
	900	0.087 ± 0.011	0.036 ± 0.011	0.42 ± 0.13
	1080	0.137 ± 0.014	$0.036 \pm 0.012^{*iv}$	0.92 ± 0.16
9	600	0.323 ± 0.019	0.154 ± 0.018	1.03 ± 0.15
	700	0.268 ± 0.015	0.145 ± 0.012	0.84 ± 0.13
10	800	0.070 ± 0.004	0.043 ± 0.004	0.204 ± 0.045
	900	0.087 ± 0.010	0.053 ± 0.006	0.277 ± 0.099
	1000	0.072 ± 0.006	0.048 ± 0.009	0.211 ± 0.096
	1080	0.072 ± 0.008	$0.050 \pm 0.010^{*iv}$	0.201 ± 0.119

i Below threshold
ii 92^o
iii 88^o
iv Includes pion background
* Extrapolated background

Because some of the parameters in equation 3 were not known precisely the following errors were assigned.

1. $\Delta\Omega$, $\pm$ 2%; this error includes inaccuracies involved in measuring the displacement of the pivot as well as the magnitude of the solid angle.

2. ΔR, $\pm$ 0.15 gm/cm^2 of copper; uncertainties in ΔR are 2% when absorber E was 5.65 gm/cm^2 and 6% when absorber E was zero.

3. N_T, $\pm$1%; it was assumed that changes in the amount of hydrogen contamination in the target gave rise to this fluctuation about the mean deuterium density.

4. N(k), $\pm$ 3%; this results from uncertainties in the absolute energy calibration of the beam, variations in the laboratory temperature and pressure which cause changes in the ion chamber response, and electronic drifts in the circuit which integrates the ion chamber response.

The veto counting rates and resolving times were such that no electronic dead time corrections were necessary. A long piece of cable inserted in series with the signal from counter #1 demonstrated that there were no counts from accidental coincidences.

IV

RESULTS

Proton counting rates, subtractions, corrections, error assignments, and results are summarized in table VI for the end point energies E_o at which the reduced data was obtained. Some data was also obtained for other end point energies and is summarized in table V in a form which shows the number of protons detected per equivalent quantum as a function of E_o. At a few points the angle was changed slightly so that the end point either did not cut into the telescope acceptance.

Results of the excitation measurements are shown in figure 6. The photon energy corresponding to each point in table III and figure 6 is that energy, k, such that one half of the protons detected at the point came from photons of energy less than k and half from photons of energy greater than k. Beneath two points of the present measurement are plots of the relative probability for a photon of a given energy to give rise to a proton detected at the point. Similar plots exist for the other points but are omitted for the sake of clarity. In order to compare the present results with those of Keck and Tollestrup (4) three points from that experiment have been placed in figure 6. Since this data was originally given at the photon energy which corresponded to the mean energy for which the detecting apparatus was sensitive, the abscissa of these points has been reduced by roughly 5 mev to conform to the present criterion. The point of the excitation curve at 375 mev was obtained by

Table VI

Column 1: Point number

Column 2: Full target counting rate; "protons" per B.I.P.

Column 3: Background counting rate; "protons" per B.I.P.*

Column 4: Absorption and scattering correction; $N_{transmitted}/N_{incident}$

Column 5: Correction for motion of pivot; $\Delta\Omega/\Delta\Omega_o$

Column 6: Center of mass differential cross section; ub/ster**

Point No.	$(C.R.)_{F.T.}$	$(C.R.)_{bkg}$	Absorption	Pivot Motion	$d\sigma/d\Omega'$
1	1.58 ± 0.14	0.20 ± 0.04	0.81 ± 0.03	1.035	$1.34^{+0.17}_{-0.23}$
2	0.71 ± 0.06	0.12 ± 0.02	0.77 ± 0.04	0.998	$0.75^{+0.08}_{-0.11}$
3	0.33 ± 0.05	0.034 ± 0.010	0.71 ± 0.04	1.033	$0.58^{+0.09}_{-0.12}$
4	0.127 ± 0.018	0.025 ± 0.009	0.64 ± 0.04	1.031	$0.27^{+0.06}_{-0.08}$
5	0.061 ± 0.010	0.011 ± 0.006	0.06 ± 0.04	1.026	$0.168^{+0.042}_{-0.060}$
6	0.026 ± 0.006	0.010 ± 0.004	0.53 ± 0.03	1.025	$0.073^{+0.032}_{-0.048}$
7	0.396 ± 0.033	0.064 ± 0.014	0.60 ± 0.04	0.968	$0.65^{+0.07}_{-0.09}$
8	0.087 ± 0.011	0.036 ± 0.011	0.42 ± 0.04	1.010	$0.28^{+0.09}_{-0.13}$
9	0.323 ± 0.035	0.154 ± 0.018	0.88 ± 0.02	0.965	$0.41^{+0.10}_{-0.14}$
10	0.087 ± 0.010	0.053 ± 0.006	0.83 ± 0.02	0.966	$0.171^{+0.057}_{-0.085}$

* Includes H_2 contribution at 60°. H_2 correction assumes $\pi^-/\pi^+ \sim 1.00 \pm 0.25$.

** Includes the following errors:

a: solid angle, $\pm$ 2%
b: ΔR, $\pm$ 2% at points 1 - 8
$\pm$ 6% at points 9 and 10
c: $N_T \pm 1\%$

Figure 6

Result of excitation measurement at 90°.

This figure is discussed in section 4.

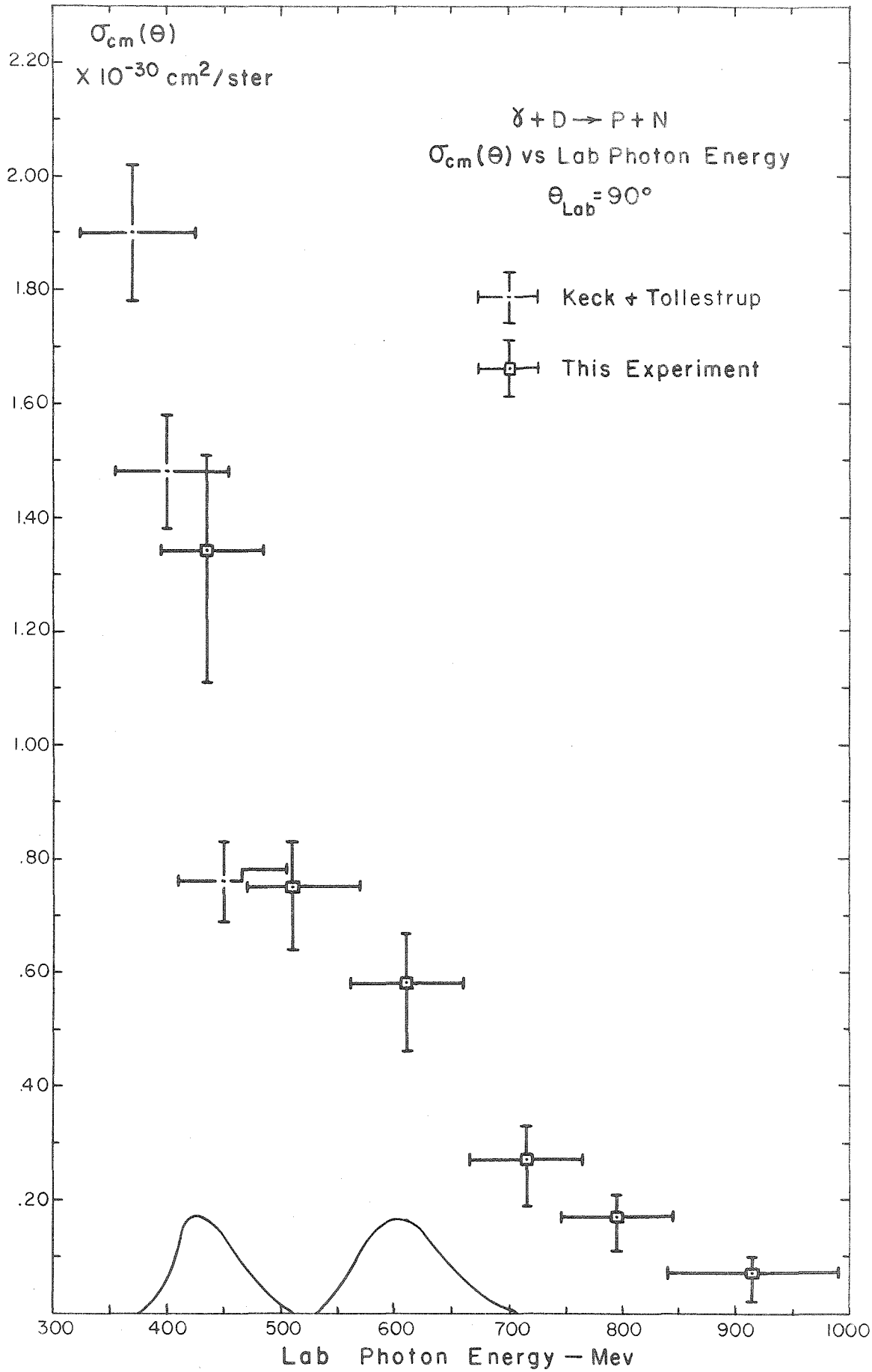
$\sigma_{cm}(\theta)$
X 10^{-30} cm^2/ster
$\gamma + D \rightarrow P + N$
$\sigma_{cm}(\theta)$ vs Lab Photon Energy
$\theta_{Lab} = 90°$
Keck + Tollestrup
This Experiment
2.20
2.00
1.80
1.60
1.40
1.20
1.00
.80
.60
.40
.20
300
400
500
600
700
800
900
1000
Lab Photon Energy — Mev

interpolation of the 93° excitation curve of Keck and Tollestrup. The horizontal error represents the photon energy interval within which lay approximately 80% of the photons which reacted to give protons detected by the telescope. The origin of the vertical error assignment is discussed in the preceding section.

In figure 7 are center of mass angular distributions at 500 and 700 mev. The plotted points in this figure were interpolated or extrapolated from the photon energy at which the measurements had actually been made. Again points from the former measurements (4) are shown for comparison. The curves through the data of Keck and Tollestrup are least squares fits to the form $A + B \cos \theta + C \cos^2 \theta$. No curves are drawn through the present angular distributions since the errors are large and there is no theoretical preference for any of the various distributions which fit the data equally well. The vertical error is obtained in the same way as in figure 6. Here the horizontal error is the angular interval in which 80% of the detected protons were emitted. Along the θ axis is a representative distribution of the relative probability of detecting a proton emitted at a given angle.

Figure 8 is the total cross section from 70 to 900 mev. Total cross sections from the present data were obtained at 500 mev by integrating a distribution similar to that obtained at 455 mev; at 700, 800, and 900 mev by assuming isotropy; and at 600 mev by integrating an angular distribution which is half way between isotropic and the one used at 500 mev. These angular distributions (although they were not necessarily the correct ones) were consistent with the

Figure 7

C. M. angular distribution.

These curves are discussed in section 4.

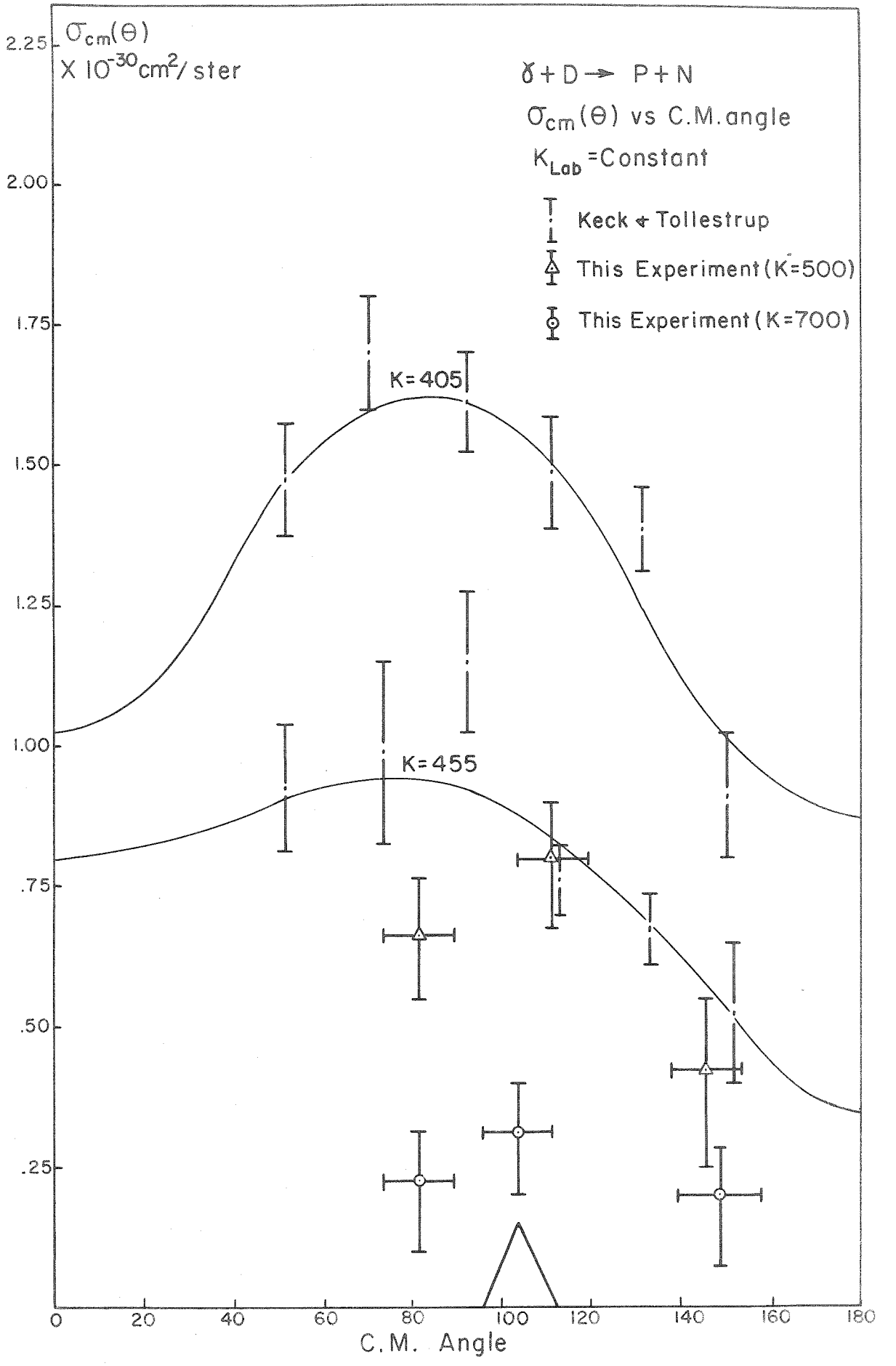
$\sigma_{cm}(\theta)$
X 10^{-30}cm^2/ster
$\gamma + D \rightarrow P + N$
$\sigma_{cm}(\theta)$ vs C.M. angle
K_{Lab} = Constant
Keck & Tollestrup
This Experiment (K=500)
This Experiment (K=700)
K=405
K=455
2.25
2.00
1.75
1.50
1.25
1.00
.75
.50
.25
0
20
40
60
80
100
120
140
160
180
C.M. Angle

Figure 8

Total elastic photodisintegration cross section from 70 to 900 mev.

This curve is discussed in section 4.

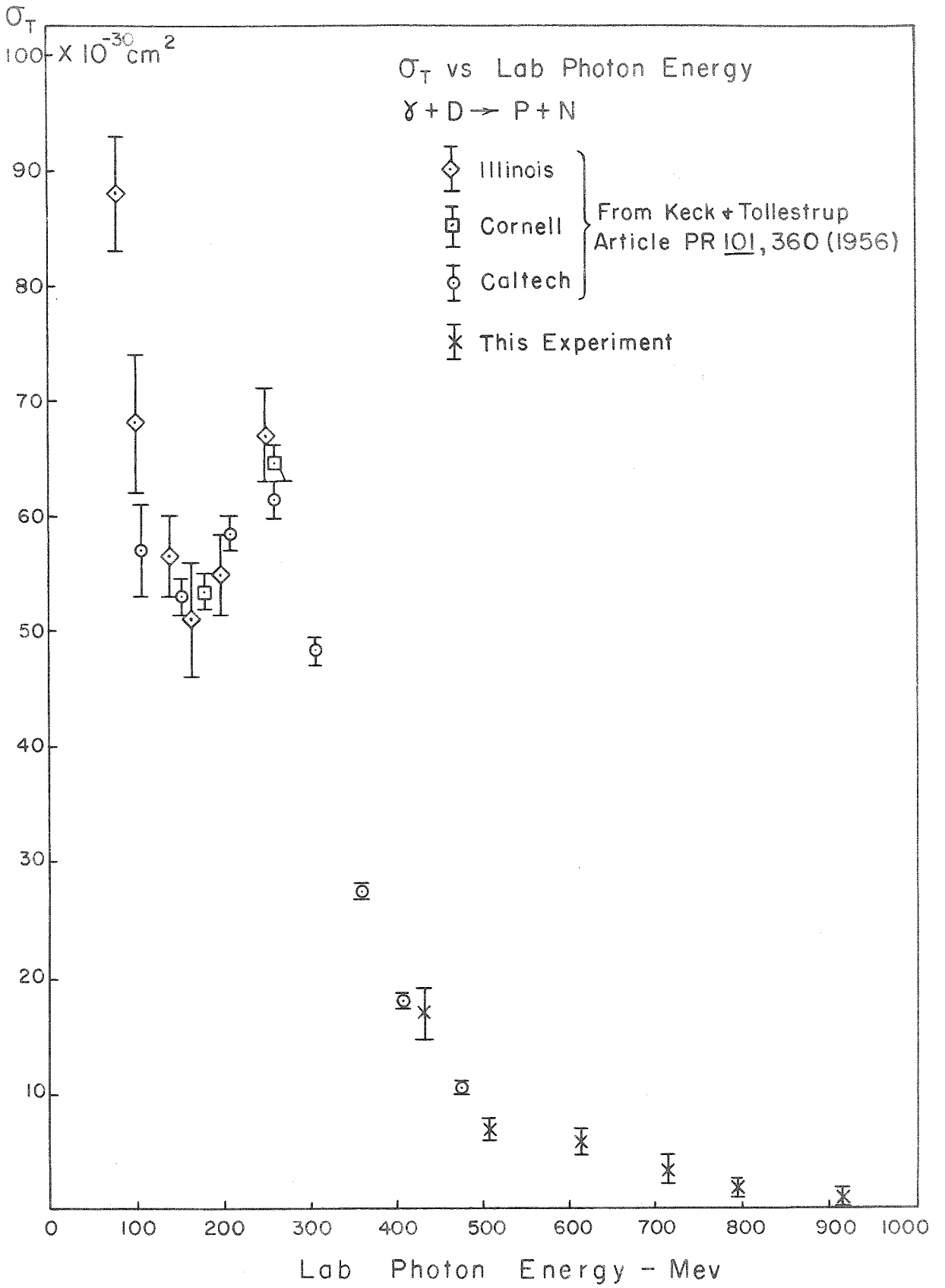
σ_T
100 X 10^{-30} cm^2
σ_T vs Lab Photon Energy
$\gamma + D \rightarrow P + N$
Illinois
Cornell
Caltech
From Keck & Tollestrup
Article PR 101, 360 (1956)
This Experiment
90
80
70
60
50
40
30
20
10
0
100
200
300
400
500
600
700
800
900
1000
Lab Photon Energy - Mev

data. The total cross section values thus obtained are within the statistical error of other reasonable assumptions concerning the angular distributions.

V

DISCUSSION

By assuming the elastic photodisintegration process to take place through intermediate states in which mesons are produced, scattered, and absorbed, Zachariasen (7) obtained qualitative agreement between his cross section calculations and experiment. These computations may be considered as a confirmation of the idea that at energies greater than 100 mev meson effects must be considered explicitly. Calculations which failed to take account of such effects were not in qualitative agreement with the magnitude or with the resonant behavior of the observations. The lack of a tractable meson theory for relativistic energies prohibits a calculation of the type made by Zachariasen in the energy region with which this experiment is concerned.

However, there exists a qualitative argument showing that the present results are reasonable. The reasoning is similar to that of Wilson (16) who explained the observations for photon energies up to 400 mev within the experimental error.

Consider that an intermediate state is formed. i.e.

$$\gamma + D \rightarrow D^* = N^* + N$$

D^* consists of one nucleon in the ground state and the other nucleon in an excited state. The probability of formation of D^* at a particular energy is proportional to the sum of all the total cross sections for single or multiple pion production from protons plus those from neutrons. This follows from the hypothesis that the magnitude of

the total meson current is not affected by the proximity of the two nucleons and that meson interactions which occur before the photon is absorbed may be neglected except in the lowest order.

The excited nucleon is likely to decay in any of the following modes:

$$N^* \rightarrow N + \pi$$
$$N + 2\pi$$
$$N + 3\pi \text{ etc.}$$

Relative frequencies of the various decay modes are determined by unknown matrix elements and the density of final states.

There is some chance that pions emitted by N^* will be absorbed before they leave the interaction volume. If these pions are absorbed the net reaction is elastic photodisintegration:

$$\gamma + D \rightarrow P + N$$

For elastic photodisintegration to occur it is necessary that when D^* is formed the proton and neutron be within an interaction volume whose dimensions are the order of the range of nuclear forces.

Combining these ideas it is possible to write an expression for the elastic photodisintegration cross section in terms of other cross sections.

Thus

$$\sigma_D = \sigma_\pi \; P(r < r_o) \; (\sigma^e_{np}/\sigma^t_{np}) \qquad (4)$$

σ_π is the cross section for single plus multiple pion production from neutron and proton.

$P(r < r_o)$ is the probability that neutron and proton are separated by a distance less than r_o when the incident radiation is absorbed. Wilson assumed r_o independent of energy and equal to $(\hbar/m_\pi c) = 1.41 \cdot 10^{-13}$ cm which yields

$P(r < r_o) = 0.11$ for a deuteron described by the Hulthen wave function. The same assumption is made in the present argument. σ^e_{np} and σ^t_{np} are respectively the elastic and total n-p cross sections for a center of mass energy equal to the corresponding center of mass energy in the photodisintegration process. $\sigma^e_{np}/\sigma^t_{np}$ gives an upper limit for the probability of elastic decay if D^* is formed when proton and neutron are initially within the interaction distance r_o. The upper limit qualification results from the fact that σ^e_{np} and σ^t_{np} include diffraction scattering contributions. For this problem it is assumed that a compound nucleus is formed and the desired quantity is the relative probability that decay will take place into the entrance channel. Therefore it is necessary to subtract the diffraction scattering contribution from σ^e_{np} and σ^t_{np}. However, the diffraction scattering accounts for almost all of σ^e_{np} with the result that the imprecise measurements of this quantity make the subtraction meaningless. The use of the measured values of σ^e_{np} and σ^t_{np} thus yield an upper limit of the ratio $\sigma^{e\text{-}ds}_{np}/\sigma^{t\text{-}ds}_{np}$ where $\sigma^{e\text{-}ds}_{np}$ and $\sigma^{t\text{-}ds}_{np}$ are respectively the elastic and total n-p cross sections minus the diffraction scattering contamination. It is in this ratio that the expression for the photodisintegration cross section is most different from that of Wilson who assumed that the matrix elements were equal for all modes of disintegration of the n-p system and therefore that the branching ratios were determined only by the available phase space. The use of total and elastic n-p cross sections takes into account the possibility that the matrix elements may be different for the various modes.

The result of substituting numbers in the expression for the cross section (equation 3) is shown in figure 9. Because of the large

Figure 9

Calculated and observed total cross sections.

This figure is discussed in section 6.

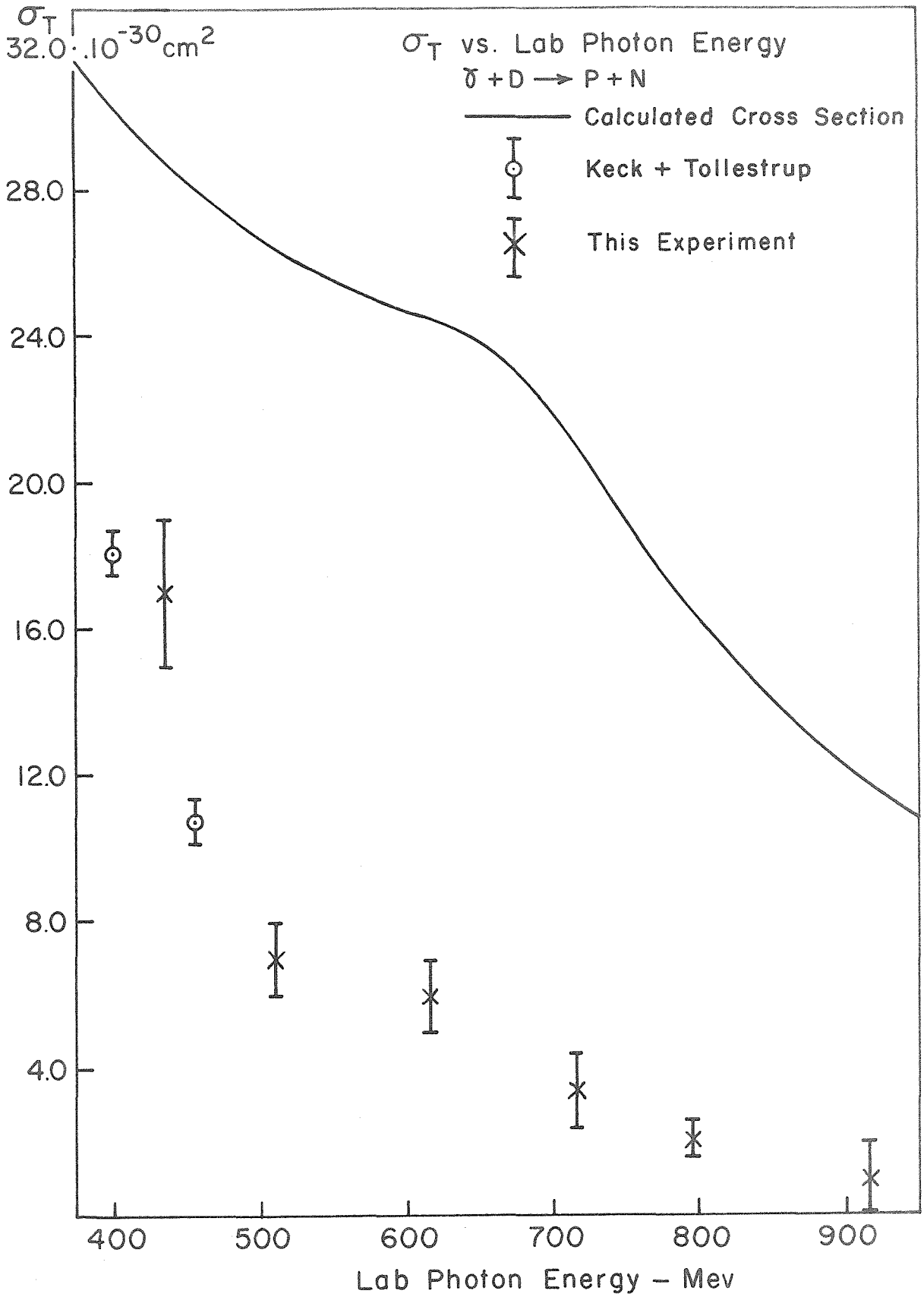
σ_T
32.0 · .10^{-30}cm^2
σ_T vs. Lab Photon Energy
$\gamma + D \rightarrow P + N$
Calculated Cross Section
Keck + Tollestrup
This Experiment
28.0
24.0
20.0
16.0
12.0
8.0
4.0
400
500
600
700
800
900
Lab Photon Energy – Mev

uncertainties in the measured and inferred quantities the standard deviations are one half the value of each plotted point on the theoretical curve. The single pion part of σ_{π} takes the values of Dixon and Walker (17), Neugebauer, Wales, and Walker (18), and Althoff and Bingham (19). The multiple pion part uses the results of Sellin (8) and assumes that the cross section for pion pairs from neutrons is the same as that from protons. The further assumption is made that pair production takes place through a pure isotopic spin state so that it is possible to relate Sellin's measurements of the charged pair cross section to other charge combinations through the use of the appropriate Clebsch-Gordon coefficients. (The latter is not essential since mixed isotopic spin states yield a similar charged to total pair ratio.) Since the n-p cross sections are very difficult to measure at high energies it was necessary to say that $\sigma^{e}_{np}/\sigma^{t}_{np} = \sigma^{e}_{pp}/\sigma^{t}_{pp}$ and thereby ignore the T=0 interaction between proton and neutron. Because the upper limit value was used for $\sigma^{e\text{-}ds}_{np}/\sigma^{t\text{-}ds}_{np}$, figure 9 yields an upper limit for the elastic photodisintegration cross section. This discussion was presented in order to indicate that the total cross sections are consistent with a Wilson-like phenomenological explanation of the process.

On the other hand it is possible to assume that a measurement of the elastic photodisintegration cross section gives the ratio $\sigma^{e\text{-}ds}_{np}/\sigma^{t\text{-}ds}_{np}$. Substitution into equation 3 leads to the following:

$E_{c.m.}$	$\sigma_{np}^{e\text{-}ds}/\sigma_{np}^{t\text{-}ds}$
350	0.30
420	0.14
480	0.105
545	0.061
600	0.048
665	0.027

Again because of the many assumptions the values of $\sigma_{np}^{e\text{-}ds}/\sigma_{np}^{t\text{-}ds}$ can be considered only as order of magnitude estimates of this quantity.

VI

SUMMARY

This experiment was useful in so far as it yielded information about the cross section for elastic photodisintegration of the deuteron in an energy region where the process had not yet been investigated. A cross section which was small both in absolute and relative magnitude limited the quantity and quality of the data that was obtained. It was necessary to collect data over a long period of time and to accept the inaccuracies inherent in separating with a counter telescope a small number of high energy protons from a flux of particles composed predominently of pions and shower products. Unless new developments are made in the telescope method it seems that additional measurements of the process by this means are not worth while. If it were decided to continue the experiment serious thought should be given to a detecting system which uses focusing and bending magnets.

From a theoretical point of view further measurements are not particularly desirable in the near future. The present experiment has shown nothing which is surprising in the behavior of the cross section. Also, there is doubt whether elastic photodisintegration experiments are an efficient means of gaining insight into the nature of meson fields. Such experiments can be used to check theories once they have been developed, but at the present time no theory, that is in general agreement with other more easily observed phenomena, has reached the point where it can either be proven or disproven by high energy elastic photodisintegration showing the general behavior found here.

APPENDIX I

The statement was made that at threshold for pion photoproduction from deuterium when the vector momentum of one of the recoil nucleons is fixed, the pion(s) and other nucleon are emitted in the laboratory with equal vector velocities. This is equivalent to saying that the pion(s) and nucleon are at rest with respect to each other. The following is a proof of the statement.

Let k = laboratory 4 momentum of photon

P_T = laboratory 4 momentum of target

P_1 = laboratory 4 momentum of nucleon whose vector momentum is fixed

P_2 = laboratory 4 momentum of other reaction products

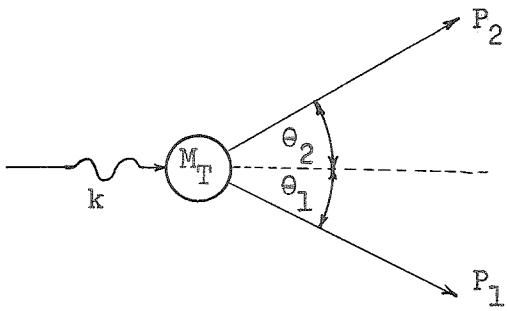

conservation of 4 momentum yields

$$k + P_T = P_1 + P_2 \tag{4}$$

$$P_2 = k + P_T - P_1 \tag{5}$$

squaring and using the fact that $P_T^2 = M_T^2$ yields

$$P_2^2 = M_2^2 = M_T^2 + M_1^2 + 2|k|(M_T - E_1) - 2M_T E_1 + 2|k||P_1|\cos\theta \tag{6}$$

$$|k| = \left[M_2^2 - M_T^2 - M_1^2 + 2M_T E_1\right] \cdot \left[2(|P_1|\cos\theta + M_T - E_1)\right]^{-1} \tag{7}$$

Equation 7 shows that for fixed p_1 the lowest photon energy at which the reaction can occur is when M_2 is minimal. Minimal M_2

means that all particles of which 5 is composed are emitted with laboratory vector velocities which are equal.

APPENDIX II

During the course of the experiment information was collected concerning the number of photoprotons produced by a high energy bremsstrahlung beam from carbon. The carbon counting rate is a function of the telescope's angular and energy apertures, number of target nuclei per square centimeter, machine end point energy, bramsstrahlung spectrum, and a differential cross section of the form $\sigma(k, T_p, \theta_p)$.

$$C.R. = N_T \frac{1.20 \cdot 10^{12} R(E_o)}{E_o} d\Omega dT_p \left[\int_o^{E_o} \sigma(k, T_p \theta_p) \frac{B(E_o, k)}{k} dk \right] \quad (8)$$

Except for the expression in the bracket the quantities in the above equation are defined as in Section F.

$\sigma^*(E_o, T_p, \theta_p) = \int_o^{E_o} \sigma(k, T_p, \theta_p) \left[B(E_o, k) dk / k \right]$ is called "yield per equivalent quantum." σ^* is tabulated in table VII. Equation 8 makes the approximation that $\sigma(k, T_p \theta_p)$ varies only linearly over the angular and energy apertures of the telescope. The data has been corrected for absorption of protons in the telescope absorber. Errors were assigned using the same criteria as was applied to the deuterium data. Column 5 of table VII is a compilation of the carbon data in the form Protons/B.I.P.-gm carbon-mev-steradian.

There have been many investigations of the mechanism by which high energy nucleons are produced in the interaction of photons with light nuclei. Experiments with bremsstrahlung end points at around 300 mev are consistent with the "pseudo deuteron" model, which explains the process by assuming that the incident radiation interacts with only two nucleons so that external to the nucleus the reaction cannot be

Table VII

Θ_p	T_p	E_o	$10^{31}\sigma^*(cm^2)$	Protons/B.I.P.-gm carbon-mev-ster
60	194	700	2.95 ± 0.41	39.6 ± 5.5
60	254	1000	1.86 ± 0.26	17.4 ± 2.4
60	279	600	0.64 ± 0.09	10.0 ± 1.4
		700	0.67 ± 0.10	8.9 ± 1.4
		800	0.79 ± 0.12	9.3 ± 1.3
		900	1.00 ± 0.14	10.4 ± 1.5
		1000	1.06 ± 0.15	10.0 ± 1.4
		1080	1.32 ± 0.19	11.4 ± 1.6
90	194	700	0.76 ± 0.11	10.2 ± 1.5
		800	0.88 ± 0.14	10.4 ± 1.6
		900	1.16 ± 0.17	12.2 ± 1.7
		1080	1.22 ± 0.18	10.6 ± 1.5
90	254	1068	0.46 ± 0.06	4.1 ± 0.6
90	279	1068	0.62 ± 0.09	5.4 ± 0.8
90	303	1068	0.19 ± 0.03	1.7 ± 0.2
130	127	600	2.24 ± 0.31	35.0 ± 4.8
		650	2.63 ± 0.37	37.8 ± 5.3
		700	2.62 ± 0.37	25.1 ± 5.0
		750	2.56 ± 0.36	32.0 ± 4.5
		800	2.81 ± 0.39	32.8 ± 4.5
		900	3.21 ± 0.45	33.6 ± 4.7
		1000	3.46 ± 0.48	32.4 ± 4.4
130	155	600	0.85 ± 0.12	13.2 ± 1.8
		700	1.13 ± 0.16	15.1 ± 2.2
		750	1.28 ± 0.18	16.0 ± 2.2
		800	1.44 ± 0.20	16.8 ± 2.4
		900	1.49 ± 0.21	15.6 ± 2.1
		1000	1.68 ± 0.24	15.7 ± 2.3

distinguished from photodisintegration of the deuteron when the deuteron initially has kinetic energy due to its motion within the nucleus. These experiments showed an angular correlation between neutron and proton which would be expected from the photodisintegration of a real deuteron (20,21). The proton angular distributions from lithium and oxygen were roughly the same as from deuterium (21) and all protons seemed to be correlated with neutrons (20). The present measurements examine photoprotons from carbon with bremsstrahlung end points ranging from 600 to 1080 mev. The results imply that the two body nature of the reaction disappears at these energies since the yield depends on the bremsstrahlung end point and the number of photoprotons cannot be accounted for by assuming the nucleus to consist of the number of deuterons implied by the low energy experiments.

The following is an explanation of the observations over the whole energy range. With the "pseudo deuteron" model the process takes place through the production and absorption of real or virtual pions with only two adjacent nucleons taking part. This is similar to the disintegration process which takes place in free deuterons, but here the probability, $P(r < r_o)$, that the two nucleons be initially within an interaction distance r_o is close to unity. At energies up to about 400 mev the probability of elastic decay of the excited system is also unity. Hence the number of proton neutron pairs which are observed for a particular photon energy should be of the order of A times the total meson cross section at that energy where A is the number of nucleons in the nucleus. This is approximately the case at the energies up to which the earlier experiments were performed.

At higher energies the probability of elastic decay should decrease. Thus the probability that mesons are emitted from the two nucleon system increases with increasing excitation energy. The mean free path in a carbon nucleus for mesons whose energy is in an interval between 100 and 900 mev is less than the nuclear diameter. Hence there is a high probability for the meson to interact before it can escape from the nucleus. High energy protons can result from the interaction of such mesons with another deuteron-like subunit or from the recoil and subsequent scattering of the nucleon off of which the meson was produced. In either case the kinematics are not characteristic of a two body interaction. An order of magnitude calculation, which made use of the simplifying assumption that all protons arise from the absorption of pions by pseudo deuterons, showed that the above ideas could account for the observed number of protons.

REFERENCES

1. J. Blatt and V. F. Weisskopf, Theoretical Nuclear Physics, John Wiley and Sons (1952).

2. Yamagata, Barton, Hanson and Smith, Phys. Rev. 95, 576, (1954); E. A. Whalin, Phys. Rev. 95, 1362 (1954); L. Allen, Jr., Phys. Rev. 98, 705 (1955)

3. Keck, Littauer, O'Neill, Perry, and Woodward, Phys. Rev. 93, 827 (1954).

4. Keck and Tollestrup, Phys. Rev. 101, 360 (1956).

5. L. I. Schiff, Phys. Rev. 78, 733 (1951).

6. J. F. Marshall and E. Guth, Phys. Rev. 78, 738 (1950).

7. F. Zachariasen, Phys. Rev. 101, 371 (1956).

8. Sellin, Cocconi, Cocconi, and Hart, Phys. Rev. 112, 1323 (1959).

9. R. Gomez, Private Communication.

10. R. R. Wilson, Nuc. Instr. 1, 101 (1957).

11. R. M. Worlock, Thesis, Cal Tech (1958).

12. E. Emery, Private Communication.

13. M. P. Ernstene, Thesis, Cal Tech (1959).

14. Richardson, Ball, Leith, and Moyer, Phys. Rev. 86, 29 (1952).

15. Chamberlain, Segre, Tripp, Wiegand, and Ypsilantis, Phys. Rev. 102, 1695 (1950).

16. R. R. Wilson, Phys. Rev. 104, 218 (1956).

17. F. P. Dixon, Thesis, Cal Tech (1960).

18. Wales, Private Communication.

19. Bingham, Private Communication.

20. Barton and Smith, Phys. Rev. 110, 1143 (1958).

21. Wattenberg, Odian, Stein, Wilson, and Weinstein, Phys. Rev. 104, 1710 (1956).